Electronic Supplementary Material (ESI) for Physical Chemistry Chemical Physics.

Supporting Information for:

Explicit solvent simulations of the aqueous oxidation potential and reorganization energy for neutral molecules: Gas phase, linear solvent response, and non-linear response contributions

Jennifer J. Guerard, Peter R. Tentscher, Marianne Seijo, and J. Samuel Arey

Table of Contents

Determination of AIE_{gas}^{ref}, VIE_{gas}^{ref}, and $NVEA_{gas}^{ref}$ values

Equilibrium gas phase geometries were minimized with B2PLYP-D,[1,2] using Aldrich's tzvpp basis set[3] augmented with diffuse functions from Dunning's aug-cc-pVTZ[4] basis set for N, O, and S atoms, with the Gaussian09 rev. B.01 software suite.[5] With these geometries, thermal contributions from translations, rigid rotations, and vibrations at 298 K (i.e., $G_{gas,ox}^{therm}(r_{ox})$ and $G_{gas,red}^{therm}(r_{red})$ in eq 6) were computed based on harmonic frequencies obtained with the same level of theory. B2PLYP-D was recently found to perform well for geometries and frequencies of gas phase radicals.[6] On these B2PLYP-D geometries, electronic contributions (i.e., $E_{gas,ox}(r_{ox})$, $E_{gas,red}(r_{red})$, $E_{gas,ox}(r_{red})$, and $E_{gas,red}(r_{ox})$ in eqs 6, 7, and 8) were determined from single point calculations on these stationary structures with the following model chemistries: W1RO[6] for aniline and methoxybenzene and W1BD[7] for DMS, imidazole, and phenol. Previous work indicates that W1 methods produce high-quality gas phase *VIE* values for several of the organic molecules studied here.[8] Vibrational contributions to the vertical gap energies ($\Delta VIE_{gas}^{vib\ avg}$ and $\Delta NVEA_{gas}^{vib\ avg}$ in eqs 7 and 8) were computed by taking the difference between VIE_{gas} values computed on solute geometries computed with B3LYP/tzvpp augmented with diffuse functions from Dunning's aug-cc-pVTZ[4] for N, O, and S atoms, and VIE_{gas} values computed on vibrationally averaged structures with the same level of theory, according to the anharmonic VPT2 protocol.[9]

Classical Molecular Mechanics (MM) Molecular Dynamics Simulations

Separate molecular dynamics trajectories were performed for the reduced neutral species and for the oxidized radical cation species of each molecule in the chemical test set. For each solute, RESP charges were computed as follows. The gas phase geometries of both the reduced and oxidized structures were optimized using M05-2X[10]/aug-cc-pVDZ[4] as implemented in Gaussian09 rev. B.01.[5] RESP[11] charges were generated from these geometries using the gas phase M05-2X/aug-cc-pVDZ electronic density. Previous literature has shown that M05-2X performs well for thermochemistry.[10] The RESP[11] charges and coordinates were then imported into the antechamber module of AMBER (v. 11)[12] and then into LEAP, whereby GAFF force field parameters[13] (atom type, Lennard-Jones parameters, bonding and angles) were generated. To introduce the solute into a solvated system, we first performed a 15 ps annealing NVT run of Na^+ ion together with 4887 POL3[14] water molecules in a cubic box having periodic boundary conditions. This was followed by a 150 ps NPT simulation to equilibrate the density at 300 K with a Langevin thermostat (γ=1 ps^{-1}) and isotropic position pressure scaling at 1 bar with 44.6×10^{-6} bar^{-1} compressibility and a pressure relaxation time of 1.0 ps. The SHAKE[15] algorithm was employed for the solvent molecules. The resulting NPT-equilibrated box had dimensions 55.13×55.13×55.13 Å. A 1.5 ns NVT simulation was then conducted. The Na^+ ion and 2-4 proximate water molecules were subsequently removed and replaced with the solute, leading to simulation systems of 4882 to 4885 waters (2 waters were removed for the insertion of DMS, 3 for imidazole, and 4 for aniline, anisole, phenol). The resulting organic solute+solvent system was then further equilibrated in Sander (implemented in AMBER) using an NVT ensemble for 150 ps (0.75 fs time step) kept at the initial system size of 55.13×55.13×55.13 Å.

Quantum Mechanical / Molecular Mechanical (QM/MM) Molecular Dynamics Simulations

For both the reduced neutral species and the oxidized radical cation species of each molecule in the test set, we performed molecular dynamics trajectories of the solvated molecule using QM/MM[16,17] molecular dynamics in an NVT ensemble with the CP2K v. 2.2.422 software[18]. The solute electronic structure was modeled with a DFT subsystem, and aqueous solvent was modeled with an MM subsystem. A QM/MM representation enabled us to capture the electronic structure of the neutral and ionized solute and also include a sufficiently large number of solvent molecules to converge the ΔVIE_{aq}[8] and $\Delta NVEA_{aq}$. This avoids the need to construct extrapolations with smaller periodic systems to estimate the effects of bulk solvent.[19]

QM/MM simulation times and system ensemble types were as follows. After an initial 150 ps pre-equilibration with a classical Hamiltonian in Sander (described in the previous section), each system was further pre-equilibrated using the QM/MM Hamiltonian in CP2K in an NVE ensemble for 5 ps. This was followed by QM/MM simulation in an NVT ensemble for 30 ps using a time step of 0.5 fs. The first 5 ps of the QM/MM NVT simulation were considered as additional pre-equilibration period and this part was discarded. The remaining 25 ps of QM/MM NVT simulation were considered as the production trajectory. Selected system geometries were extracted from the production trajectory and used to compute vertical gap energies with the EOM-IP-CCSD/6-31+G(d)/EFP model chemistry (described in the main text).

The QM/MM method protocol was as follows. The solute was represented quantum mechanically using BLYP-D2[20] with the TZV2P-GTH basis set.[21,22] The QUICKSTEP algorithm was used for the QM subsystem,[23] with orbital transformation[24] applied. For open shell species, restricted open-shell Kohn-Sham (ROKS) and self-interaction correction (SIC)[25] with values of a=0.2 and b=0.0[25] were applied to the unpaired electron. Periodic boundary conditions (PBC) were maintained with the Ewald Poisson solver.[26,27] A 13.43 Å cubic QM box surrounded the solute. These box sizes ensured a minimum distance of 2 Å between the box edges and all solute nuclei; this distance was chosen so that the total potential energy was converged to within 0.005 a.u. variation, and the energy of the QM region determined from the QUICKSTEP algorithm from a single point computation was converged to within 0.005 a.u. (data not shown). The plane wave cutoff energy was 300 Rydberg, which ensured that the QUICKSTEP energy was converged to within 0.00003 a.u. based on convergence tests systematically increasing the cutoff every 20 Ry from 240 to 480 Ry. The algorithm employed by QUICKSTEP avoids “ringing” that can occur when using BLYP without a very large cutoff.[23] Water molecules were represented with a classical, polarizable POL3 force field.[14] Polarizable water models have been shown to give good results for modeling electron transfer reactions,[28-31] However it remains unclear to us whether CP2K treats the resulting QM/MM interactions as fully mutually polarizable. The trajectories of the fixed-geometry water molecules of the classical subsystem were handled using the SHAKE algorithm. An Ewald value of 57 grid points was applied. With this GMAX value, the total MM energy was found to be converged to within 0.0001 a.u., based on several computed single-point energies of increasing GMAX values applied to a single geometry frame of the system. The coupling between the QM and MM systems is described elsewhere.[17] For QM/MM simulations conducted in the NVT ensemble, separate thermostats were applied for each the QM and MM subsystems. Each was a three-chain Nosé-Hoover thermostat[32] that maintained a temperature at 300 K with a time constant of 1000 fs. System thermal equilibrium was determined by monitoring the total system energy and confirming that the cumulative average total energy converged to within a tolerance of 1% of the system kinetic energy. In addition, the stabilities of the overall system temperature, QM region temperature, and total system potential energy were monitored.

Determination of AIE_{aq}^{TI} and AIE_{aq}^{FEP}

We conducted thermodynamic integration[33] of the free energy of oxidation using a classical Hamiltonian as implemented in AMBER. Thermodynamic integration is performed as a stepwise change in the total charge of the solute, η, through a linear combination of the potential energies (U) of the initial and final states:[34]

$$U(\eta) = (1-\eta)U_0 + \eta U_1 \tag{S1}$$

$$\Delta G_{TI} = \int_0^1 d\eta \left\langle \partial U / \partial \eta \right\rangle_\eta \approx \sum_{i=1}^{n} w_i \left\langle \partial U / \partial \eta \right\rangle_{\eta_i}, \tag{S2}$$

where η_i are intermediate charge parameter values and w_i are their respective quadrature weights. Assigning the reduced system as the initial state (U_0) and the oxidized system as the final state (U_1), we performed classical trajectories of 3 ns each, applying sequentially increasing η_i values of 0.00, 0.04691, 0.23076, 0.5, 0.76923, 0.95308, and 1.00,[12] where $\eta_i = 0$ refers to the reduced state of the solute, and $\eta_i = 1$ corresponds to the oxidized state of the solute. To apply eq 25, the η_i parameter was used mix the RESP charges of the reduced solute with those of the oxidized solute. However only the reduced solute geometry parameters were used for all reduced, oxidized, and intermediate charge simulations. This is consistent with the interpretation that eq 24 provides a determination of only the solvent contribution to non-linear response (the gas phase non-linear response component is zero, since the solute geometric parameters remain unchanged throughout the TI procedure). The term $\langle \partial U / \partial \eta \rangle_{\eta_i}$ represents the value of the numerical derivative $\partial U / \partial \eta$, evaluated at η_i, averaged over the course of the molecular dynamics trajectory. Each trajectory contained the solute and 4884 or 4885 water molecules in a 55.13 Å periodic cubic box. Force field parameters for the solute and water molecules are described in the previous section. Previous work has shown that the GAFF force field with RESP charges predicts solvation free energies of small organic molecules with typical errors of 1-2 kcal/mol, depending on the compound type.[35] In the present work, we did not rely on the GAFF to produce accurately computed total free energies of solvation, but we assumed that this approach would approximately capture the small non-linear response contribution to the solvation free energy. Trajectories were simulated using a 1 fs time step, employing the SHAKE algorithm and a Langevin thermostat (γ=1 ps^{-1}) at 300 K in an NVT ensemble. Finally, the classical analogue of linear response, the free energy perturbation result (AIE_{aq}^{FEP}), employs only $\eta = 1$ and $\eta = 0$ states:

$$AIE_{aq}^{FEP} = \left\langle \partial U / \partial \eta \right\rangle_{\eta=1} - \left\langle \partial U / \partial \eta \right\rangle_{\eta=0} \qquad \text{(S3)}$$

Implicit solvent model computations

As a point of comparison to E_{ox} values obtained with the explicit solvent approach, we also computed E_{ox} values using a competitive implicit solvent model, SMD.[36] Benchmark geometry optimized structures (detailed above, "Gas phase ionization energies") were used to compute the oxidation potential of the compounds in aqueous solution. The free energy of oxidation was determined via a thermodynamic cycle (Figure S1). The aqueous adiabatic free energy of oxidation, AIE_{aq}^{ref}, is expressed as the sum of the gas phase adiabatic ionization energy, AIE_{gas}^{ref}, and the change in free energy of solvation upon oxidation, $\Delta\Delta G_{solv}$ (eq 18). The implicit model estimate of $\Delta\Delta G_{solv}$ was obtained as the difference in solvation free energies of the oxidized and reduced species, determined with M06-2X[37]/aug-cc-pVTZ[4]/SMD in Gaussian09. M06-2X was previously shown to perform well for the computation of gas phase ionization potentials and also for oxidation potentials in aqueous solution with SMD, for small aromatic compounds.[38] Also accounted for is the conversion from the 1 atm gas phase standard state to 1 M aqueous standard state (1.89 kcal/mol, or 0.0820 eV), which cancels out due to the fact that the same number of molecular species are present on both sides of the oxidation reaction (Figure 1).[39]

Example CP2K input parameters used for the QM/MM molecular dynamics trajectory for imidazole•+

```
&EXT_RESTART
  RESTART_FILE_NAME filename-1.restart
&END EXT_RESTART

&GLOBAL
  PROJECT filename
  RUN_TYPE MD
  PRINT_LEVEL MEDIUM
&END GLOBAL

&MOTION
  &MD
    ENSEMBLE NVT
    STEPS 100 (after 5 ps equilibration phase, ran production run in series of 500 runs of 100 steps each for a total of 50,000 steps – 25 ps)
    TEMPERATURE 300
    TIMESTEP 0.5
    &THERMOSTAT
      REGION DEFINED
      &DEFINE_REGION
        MM_SUBSYS MOLECULAR
      &END DEFINE_REGION
      &DEFINE_REGION
        QM_SUBSYS MOLECULAR
      &END DEFINE_REGION
      TYPE NOSE
      &NOSE
        TIMECON 1000
      &END NOSE
    &END THERMOSTAT
  &END MD
  &CONSTRAINT
     CONSTRAINT_INIT
     SHAKE_TOLERANCE 1.0E-12
     &G3x3
       DISTANCES 1.89035 1.89035 3.0869
       MOLECULE  molecule-index
       ATOMS 1 2 3
       EXCLUDE_QM
     &END G3x3
     etc etc.
     &LAGRANGE_MULTIPLIERS OFF
     &END LAGRANGE_MULTIPLIERS
  &END CONSTRAINT
&END MOTION

&FORCE_EVAL
  METHOD QMMM
  &DFT
    CHARGE 1 (for •+)
    MULTIP 2 (for •+)
    ROKS (for open shell only)
    &MGRID
      COMMENSURATE
      CUTOFF 300
    &END MGRID
    &SIC (for open shell only)
      SIC_METHOD MAURI_US
      SIC_SCALING_A 0.2
      SIC_SCALING_B 0.0
    &END SIC
    &QS
    &END QS
    &SCF
      SCF_GUESS RESTART
      MAX_SCF 20
      EPS_SCF 1.0000E-06
      &OUTER_SCF
        EPS_SCF 20
        MAX_SCF 1.0000E-06
      &END OUTER_SCF
      &OT
        ROTATION
      &END OT
    &END SCF
    &XC
      &VDW_POTENTIAL
        POTENTIAL_TYPE PAIR_POTENTIAL
        &PAIR_POTENTIAL
          REFERENCE_FUNCTIONAL BLYP
          TYPE DFTD2
          VERBOSE_OUTPUT
          R_CUTOFF 6.5
```

```
       &END PAIR_POTENTIAL
     &END VDW_POTENTIAL
     &XC_FUNCTIONAL BLYP
     &END XC_FUNCTIONAL
   &END XC
  &END DFT
  &MM
    &FORCEFIELD
IGNORE_MISSING_CRITICAL_PARAMS
      PARMTYPE AMBER
      PARM_FILE_NAME filename.top
    &END FORCEFIELD
    &POISSON
      PERIODIC XYZ
      &EWALD
        EWALD_TYPE SPME
        ALPHA 0.2917
        GMAX 57 57 57
      &END EWALD
    &END POISSON
  &END MM
  &QMMM
    E_COUPL GAUSS
    USE_GEEP_LIB 7
    &CELL
      ABC 13.425
      PERIODIC XYZ
    &END CELL
    &PERIODIC
      GMAX 1.0
      &MULTIPOLE
        RCUT [angstrom] 6.7125
        ANALYTICAL_GTERM
      &END MULTIPOLE
    &END PERIODIC
    &FORCEFIELD
    &END FORCEFIELD
    QM_KIND C
      MM_INDEX 1 3 7
    &END QM_KIND
    &QM_KIND H
      MM_INDEX 2 4 6 8
    &END QM_KIND
    &QM_KIND N
      MM_INDEX 5 9
    &END QM_KIND
    &MM_KIND H
      RADIUS 0.31
    &END MM_KIND
    &MM_KIND O
      RADIUS 0.66
    &END MM_KIND

  &END QMMM
  &SUBSYS
   &CELL
     ABC 55.131 55.131 55.131
     PERIODIC XYZ
   &END CELL
   &TOPOLOGY
     COORD_FILE_FORMAT XYZ
     COORD_FILE_NAME filename.xyz
     CONN_FILE_FORMAT AMBER
     CONN_FILE_NAME filename.top
   &END TOPOLOGY
   &KIND H
     BASIS_SET TZV2P-GTH
     POTENTIAL GTH-BLYP-q1
    &END KIND
    &KIND N
     BASIS_SET TZV2P-GTH
     POTENTIAL GTH-BLYP-q5
    &END KIND
   &KIND C
     BASIS_SET TZV2P-GTH
     POTENTIAL GTH-BLYP-q4
   &END KIND
   &KIND O
     BASIS_SET TZV2P-GTH
     POTENTIAL GTH-BLYP-q6
   &END KIND
   &KIND S
     BASIS_SET TZV2P-GTH
     POTENTIAL GTH-BLYP-q6
   &END KIND&END SUBSYS
```

$\Delta NVEA_{aq}$ results for phenol: comparison of the present study with Ghosh et al.[40]

In both the present study and in Ghosh et al.[40], the aqueous vertical energy gap of phenol was computed with EOM-IP-CCSD and surrounding waters were modeled with effective fragment potentials. However, our $\Delta NVEA_{aq}$ value of -4.14 eV for the oxidized phenol cation differs substantially from the value of approximately -4.75 eV report by Ghosh et al. In the two studies, different algorithms were used to generate the solvated structures. We used a molecular dynamics trajectory generated with a QM/MM Hamiltonian, whereas Ghosh et al. used an entirely classically generated trajectory utilizing ENZYMIX parameters and charges generated from NBO analysis. The present study also used a larger periodic box (55 Å) compared to the previous paper (35 Å). However, other studies of box size extrapolations[41,42] show that the Helmholtz free energy of oxidation has little dependence on box size for the large box sizes used here and used by Ghosh et al. Thus it is unlikely that the observed $\Delta NVEA_{aq}$ difference of 0.6 eV can be explained by differences in box size. Other differences between the two studies include boundary conditions employed during the MD simulations and the lengths of the MD trajectories. However, we surmise that these technical differences are unlikely to explain the observed difference in the $\Delta NVEA_{aq}$. In summary, we conclude that the 0.6 eV discrepancy in $\Delta NVEA_{aq}$ reported by us and by Ghosh et al. arises from the choice of Hamiltonian that was used for the molecular dynamics trajectory.

	Aniline	Methoxy-benzene	DMS	Imidazole	Phenol
$\Delta AIE_{gas}^{non-LR}$	-0.05	-0.01	-0.10	-0.04	-0.02
$VIE_{gas}^{EOMIPCCSD}$	7.62	8.07	8.35	8.81	8.35
$NVEA_{gas}^{EOMIPCCSD}$	7.08	7.61	8.24	8.30	7.92
$AIE_{gas}^{EOMIPCCSD}$	7.35	7.84	8.29	8.55	8.14

Table S1. Gas phase EOM-IP-CCSD values determined from reference gas phase geometries with EOM-IP-CCSD/6-31+G(d) including thermal contributions from the VPT2 vibrationally averaged structures at the same level of theory for VIE_{gas}, $NVEA_{gas}$, and AIE_{gas}. $\Delta AIE_{gas}^{non-LR}$ is determined as the difference between eq. 6 and eq. 16. $VIE_{gas}^{EOMIPCCSD}$ and $NVEA_{gas}^{EOMIPCCSD}$ are determined as from eq. 7 and eq 8, and $AIE_{gas}^{EOMIPCCSD}$ is determined from eq. 16, but at the EOM-IP-CCSD/6-31+G(d) level of theory.

$$\begin{tikzcd}
D_{gas,red,(r_{red})} \arrow[r, "AIE_{gas}^{ref}"] \arrow[d, "\Delta G_{solv,A,red,(r_{red})}"] & D_{gas,ox,(r_{ox})} \arrow[d, "\Delta G_{solv,A,ox,(r_{ox})}"] & + & e^{-}_{gas} \arrow[d, "\Delta G = 0"] \\
D_{aq,red,(r_{red})} \arrow[r, "AIE_{aq}^{ref,SMD}"] & D_{aq,ox,(r_{ox})} & + & e^{-}_{gas}
\end{tikzcd}$$

Figure S1. Thermodynamic cycle for the aqueous adiabatic ionization energy (AIE_{aq}) at 298 K, employed for implicit solvent model. AIE_{gas}^{ref} was determined with eq. 6, and $AIE_{aq}^{ref,SMD}$ was determined as the sum of AIE_{gas}^{ref} and $\Delta\Delta G_{solv}^{SMD}$ computed by SMD/M06-2X/aug-cc-pVTZ.

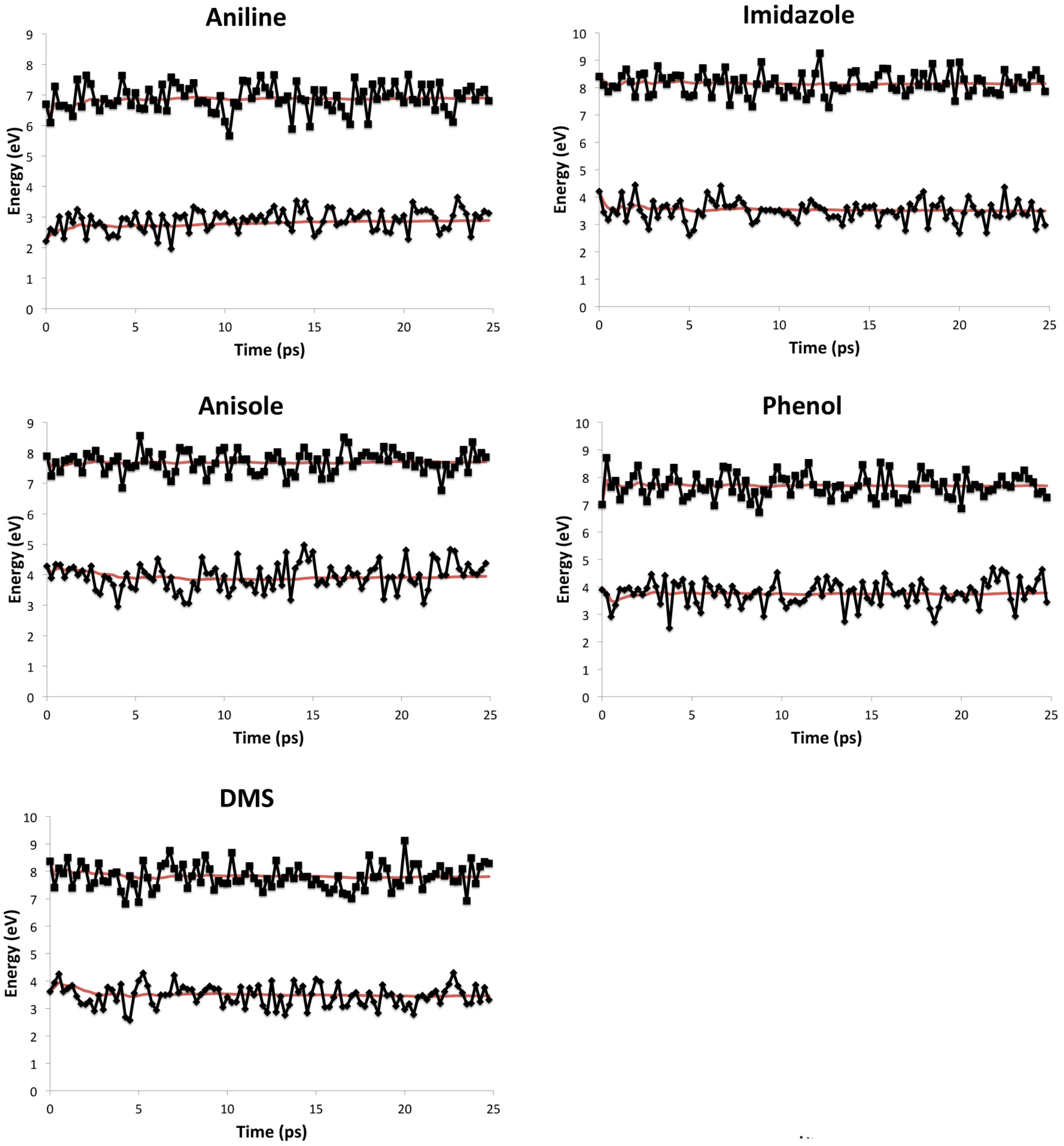

Figure S2. Times series of vertical gap energies over each 25 ps trajectory of the explicitly solvated systems, in eV. In each plot, the upper series corresponds to the VIE_{aq}, and the lower series corresponds to the $NVEA_{aq}$. Each plot shows 100 snapshots, separated by 0.25 ps each. Vertical gap energies were computed using EOM-IP-CCSD/6-31+G(d) to model the solute and using effective fragment potentials to model the cluster of 3072 water molecules.

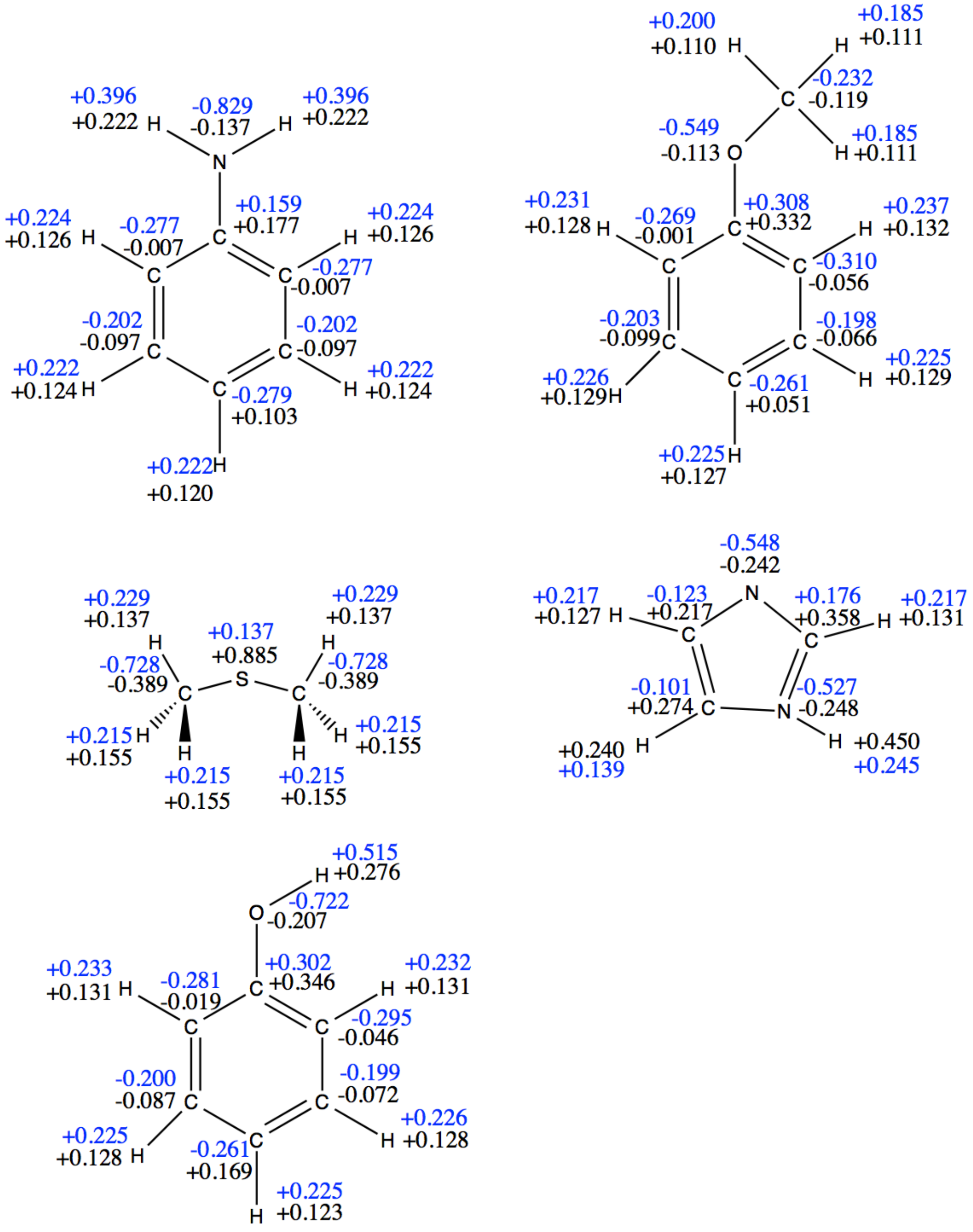

Figure S3. NPA charges on each atom for the five molecules in the test set, computed using (RO)M06-2X/aug-cc-pVTZ/SMD on B2PLYP-D geometries. Blue values represent charges on the neutral reduced species; black values represent charges on the radical oxidized species.

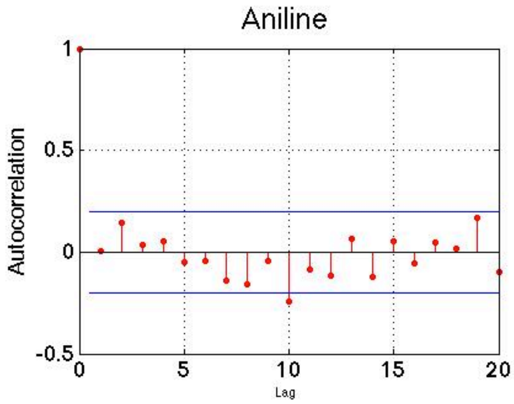
Aniline
Autocorrelation
1
0.5
0
-0.5
0
5
10
15
20
Lag

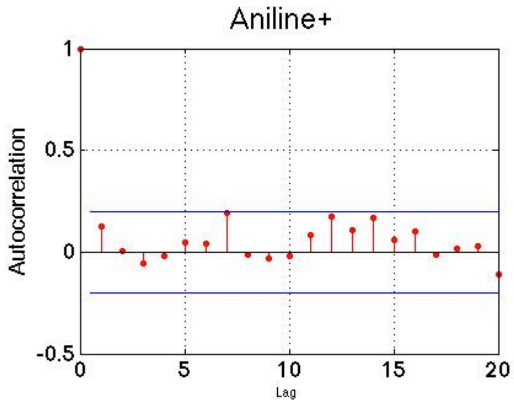
Aniline+
Autocorrelation
1
0.5
0
-0.5
0
5
10
15
20
Lag

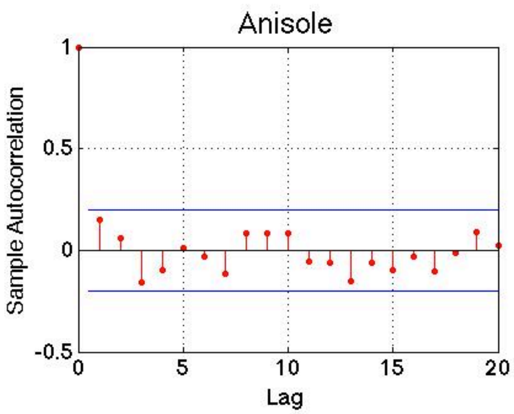
Anisole
Sample Autocorrelation
1
0.5
0
-0.5
0
5
10
15
20
Lag

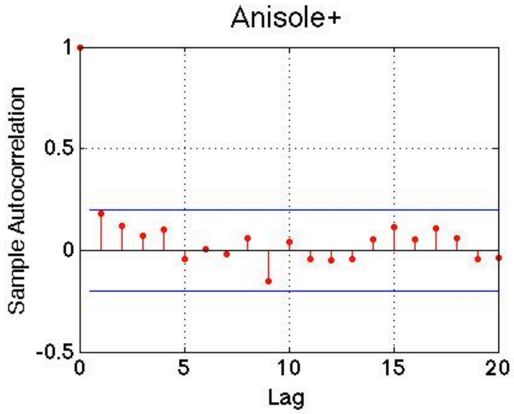
Anisole+
Sample Autocorrelation
1
0.5
0
-0.5
0
5
10
15
20
Lag

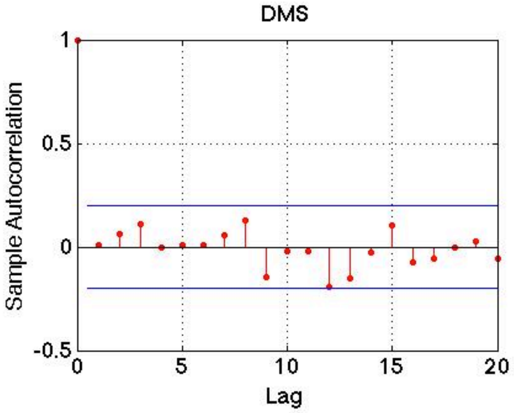
DMS
Sample Autocorrelation
1
0.5
0
-0.5
0
5
10
15
20
Lag

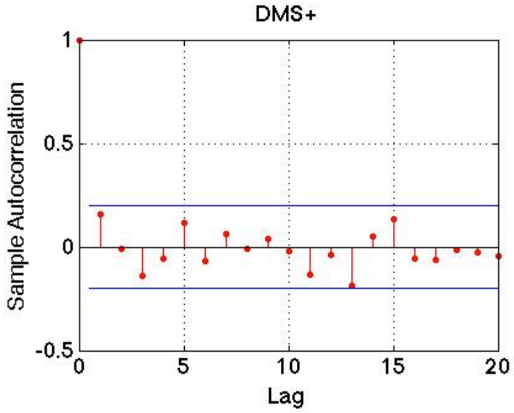
DMS+
Sample Autocorrelation
1
0.5
0
-0.5
0
5
10
15
20
Lag

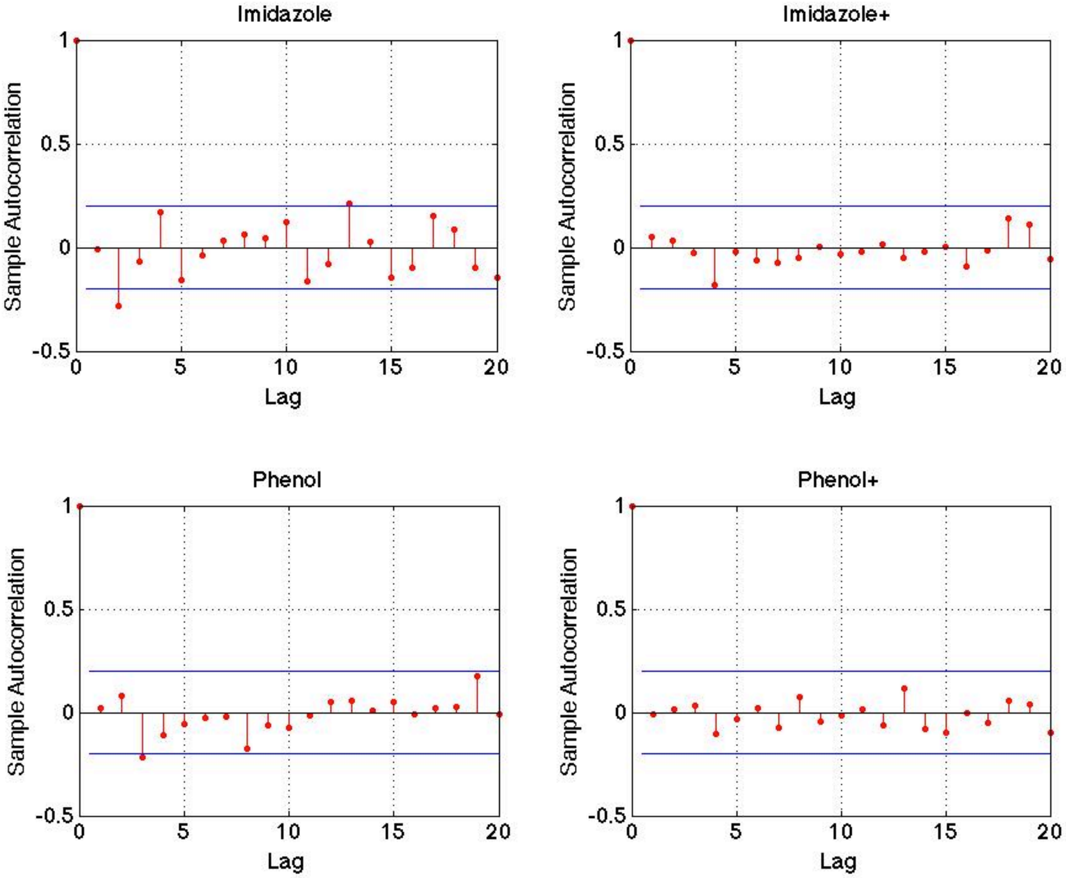

Figure S4. Plot of the sample autocorrelation function for vertical gap energy values computed from 100 snapshots taken at 0.25 ps intervals, used to test whether the sampling interval is wide enough to generate a statistically independent set of vertical gap energy values.

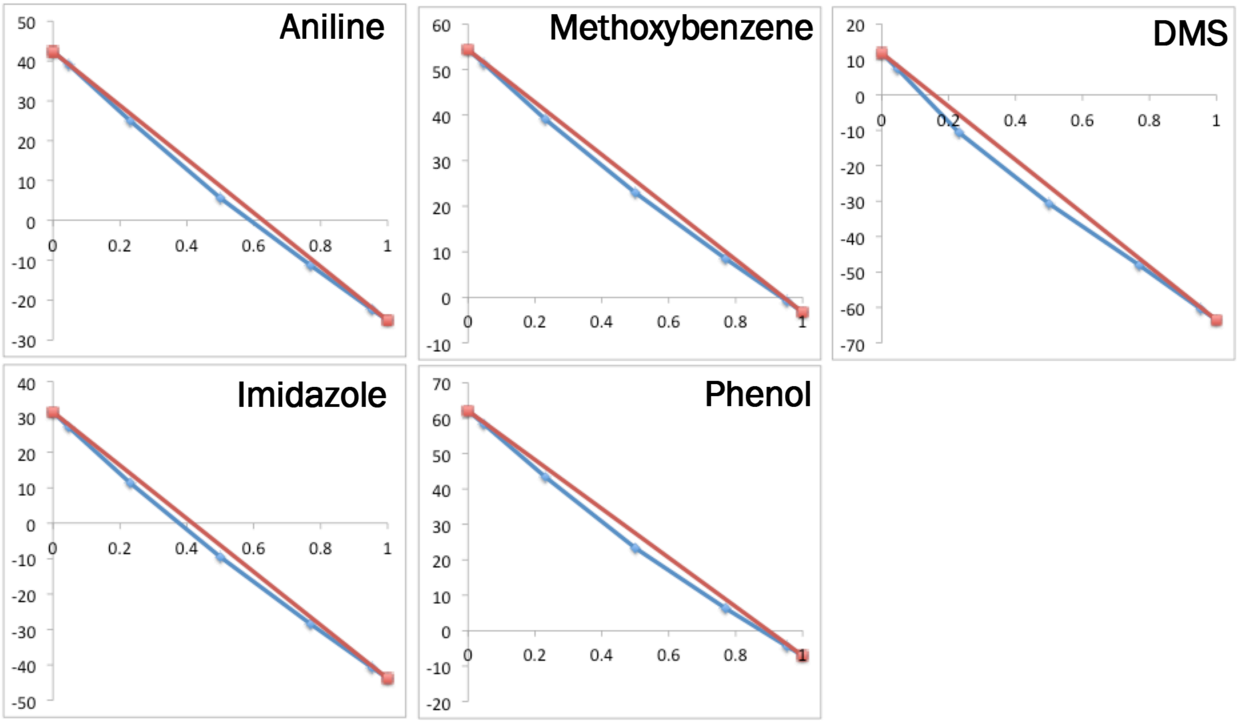

Figure S5. Classically generated free energy perturbation and thermodynamic integration curves. Red lines indicate the free energy perturbation (LRA) result, and blue lines indicate the free energy curves by thermodynamic integration.

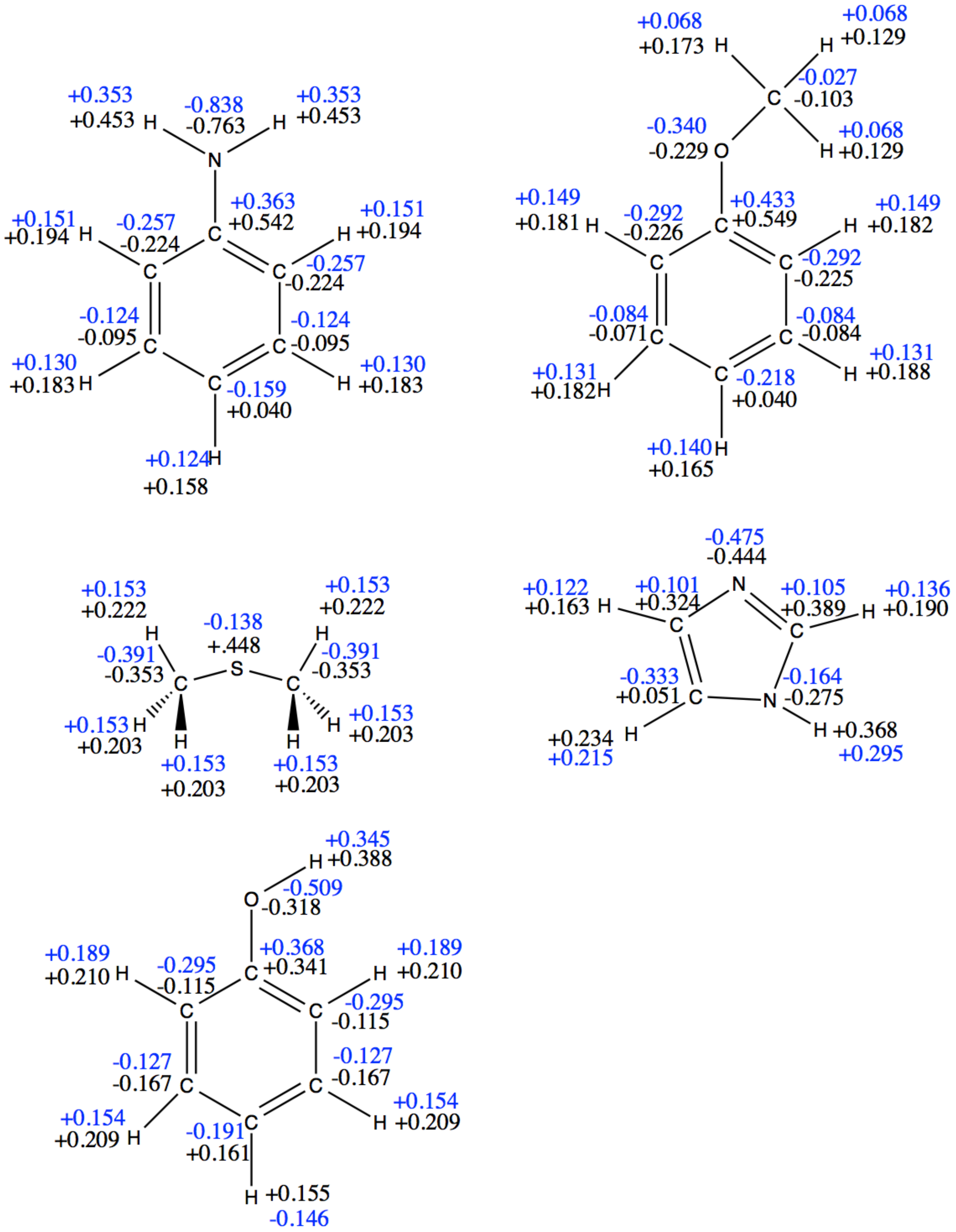

Figure S6. RESP charges on each atom on the five molecules in the test set, computed using (RO)M05-2X/aug-cc-pVDZ with B2PLYP-D geometries. Blue values represent charges on the neutral reduced species; black values represent charges on the radical oxidized species.

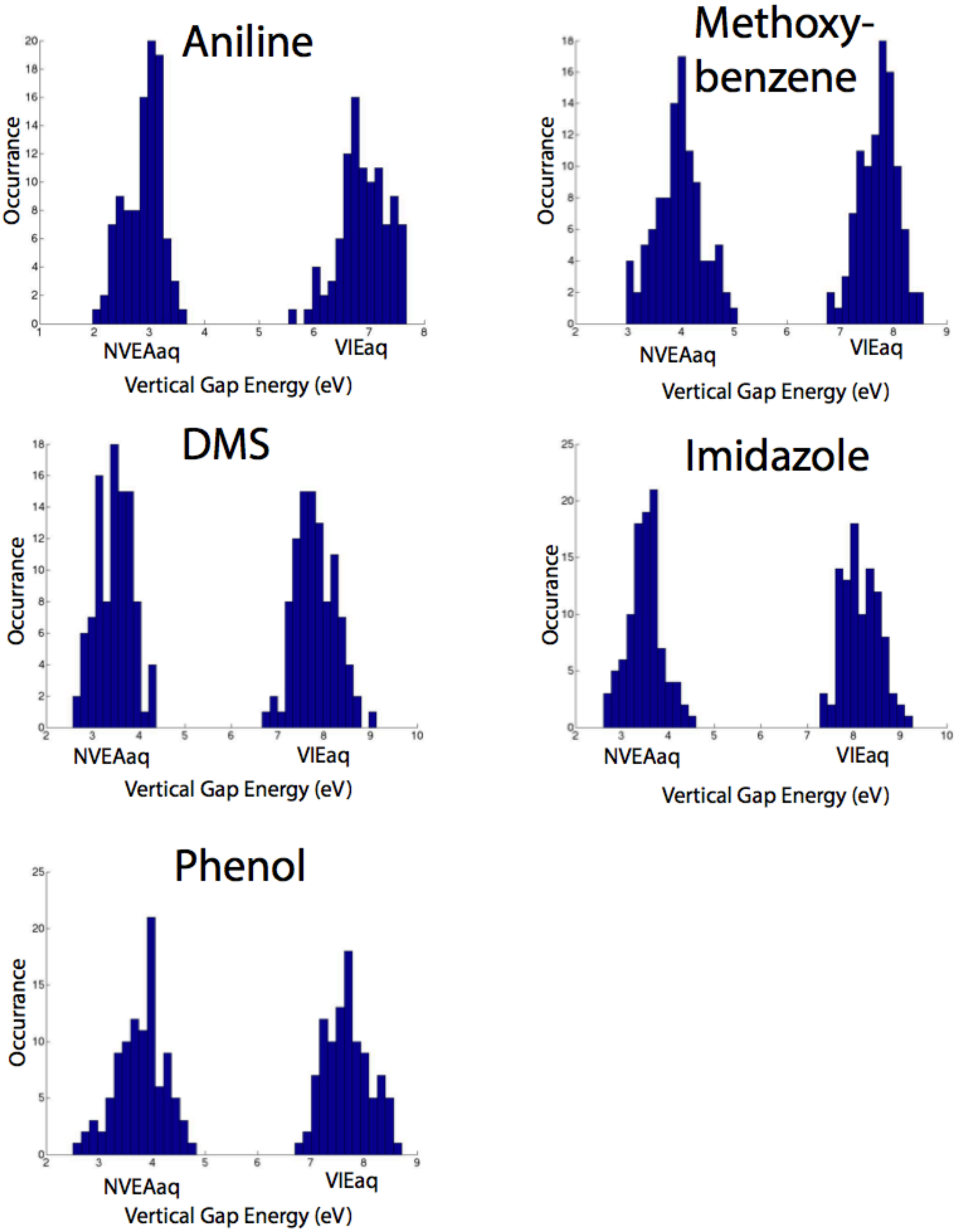

Figure S7. Histograms of vertical gap energies computed by EOM-IP-CCSD/6-31+G(d) from 100 snapshots of explicitly solvated clusters containing the solute and 3072 waters.

A1

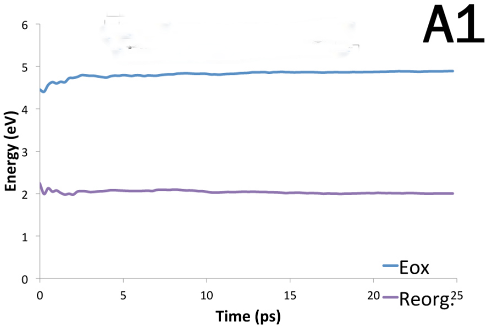

B1

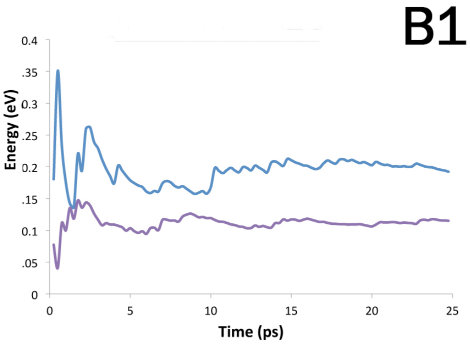

A2

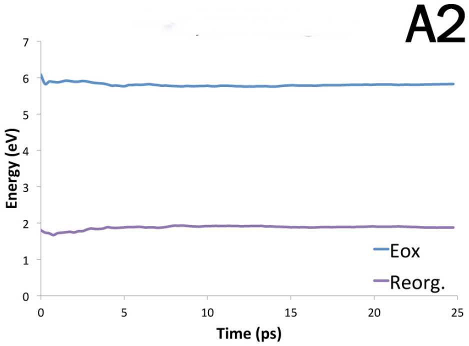

B2

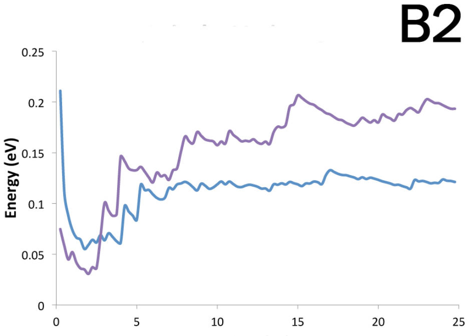

A3

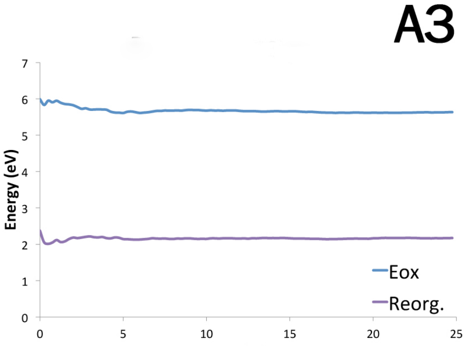

B3

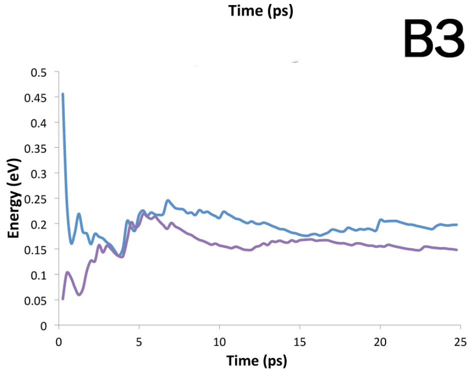

A4

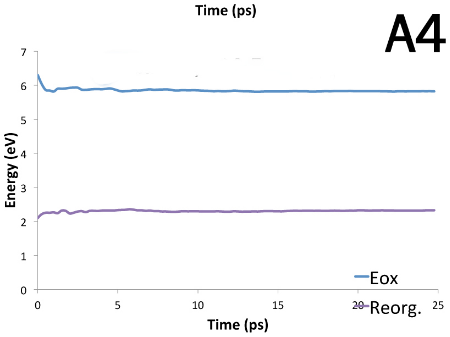

B4

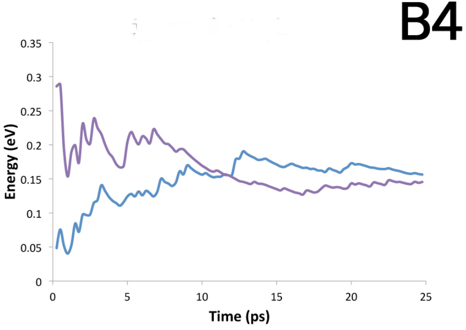

A5

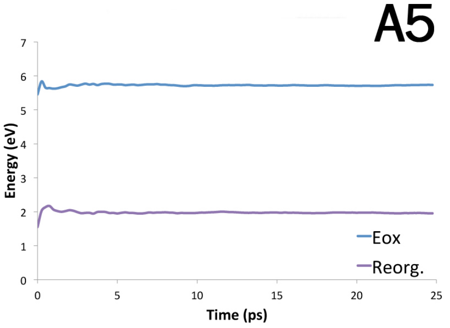

B5

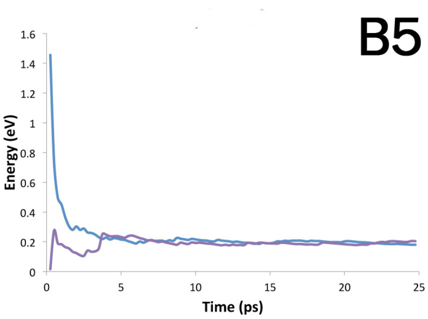

Figure S8. A1-5. Convergence of the E_{ox} value (blue) and the λ value (purple) as computed by the cumulative average of the VIE_{aq} over the course of the simulation. B1-5. Convergence of the variance of the VIE_{aq} values over the course of the simulation, where *VIE*s were computed using 100 snapshots taken at 0.25 ps intervals with EOM-IP-CCSD/6-31+G(d) to model the solute and using EFPs to model explicit waters. 1: Aniline. 2: Methoxybenzene. 3: Dimethylsulfide. 4: Imidazole. 5: Phenol.

References

1. T. Schwabe and S. Grimme, *Phys. Chem. Chem. Phys.*, 2007, **9**, 3397–3406.
2. S. Grimme, *J. Chem. Phys.*, 2006, **124**, 034108–034108–16.
3. F. Weigend and R. Ahlrichs, *Phys. Chem. Chem. Phys.*, 2005, **7**, 3297–3305.
4. R. A. Kendall, T. H. Dunning, and R. J. Harrison, *J. Chem. Phys.*, 1992, **96**, 6796–6806.
5. M. J. Frisch, G. W. Trucks, H. B. Schlegel, G. E. Scuseria, M. A. Robb, J. R. Cheeseman, G. Scalmani, V. Barone, B. Mennucci, G. A. Petersson, H. Nakatsuji, M. Caricato, X. Li, H. P. Hratchian, A. F. Izmaylov, J. Bloino, G. Zheng, J. L. Sonnenberg, M. Hada, M. Ehara, K. Toyota, R. Fukuda, J. Hasegawa, M. Ishida, T. Nakajima, Y. Honda, O. Kitao, H. Nakai, T. Vreven, J. A. Montgomery Jr., J. E. Peralta, F. Ogliaro, M. Bearpark, J. J. Heyd, E. Brothers, K. N. Kudin, V. N. Staroverov, R. Kobayashi, J. Normand, K. Raghavachari, A. Rendell, J. C. Burant, S. S. Iyengar, J. Tomasi, M. Cossi, N. Rega, J. M. Millam, M. Klene, J. E. Knox, J. B. Cross, V. Bakken, C. Adamo, J. Jaramillo, R. Gomperts, R. E. Stratmann, O. Yazyev, A. J. Austin, R. Cammi, C. Pomelli, J. W. Ochterski, R. L. Martin, K. Morokuma, V. G. Zakrzewski, G. A. Voth, P. Salvador, J. J. Dannenberg, S. Dapprich, A. D. Daniels, Ö. Farkas, J. B. Foresman, J. V. Ortiz, J. V. Cioslowski, and D. J. Fox, *Gaussian 09,* Gaussian, Inc., Wallingford CT, 2009.
6. J. M. L. Martin and G. de Oliveira, *J. Chem. Phys.*, 1999, **111**, 1843–1856.
7. P. R. Tentscher and J. S. Arey, *J. Chem. Theory Comput.*, 2012, **8**, 2165–2179.
8. P. R. Tentscher, R. Seidel, B. Winter, J. J. Guerard, and J. S. Arey, *J. Phys. Chem. B*, 2015, **119**, 238–256
9. V. Barone, *J. Chem. Phys.*, 2005, **122**, 014108.
10. Y. Zhao, N. E. Schultz, and D. G. Truhlar, *J. Chem. Theory Comput.*, 2006, **2**, 364–382.
11. C. I. Bayly, P. Cieplak, W. D. Cornell, and P. A. Kollman, *J. Phys. Chem.*, 1993, **97**, 10269–10280.
12. D. A. Case, T. A. Darden, T. E. Cheatham, C. L. Simmerling, J. Wang, R. E. Duke, R. Luo, R. C. Walker, W. Zhang, K. M. Merz, B. Roberts, B. Wang, S. Hayik, A. Roitberg, G. Seabra, I. Kolossváry, K. F. Wong, F. Paesani, J. Vanicek, J. Liu, X. Wu, S. R. Brozell, T. Steinbrecher, H. Gohlke, Q. Cai, X. Ye, M.-J. Hsieh, G. Cui, D. R. Roe, D. H. Mathews, M. G. Seetin, C. Sagui, V. Babin, T. Luchko, S. Gusarov, A. Kovalenko, and P. A. Kollman, *AMBER 10*, University of California, San Francisco, 2010.
13. J. Wang, R. M. Wolf, J. W. Caldwell, P. A. Kollman, and D. A. Case, *J. Comput. Chem.*, 2004, **25**, 1157–1174.
14. J. W. Caldwell and P. A. Kollman, *J. Phys. Chem.*, 1995, **99**, 6208–6219.

15. J.-P. Ryckaert, G. Ciccotti, and H. J. C. Berendsen, *J. Comp. Phys.*, 1977, **23**, 327–341.
16. T. Laino, F. Mohamed, A. Laio, and M. Parrinello, *J. Chem. Theory Comput.*, 2006, **2**, 1370–1378.
17. T. Laino, F. Mohamed, A. Laio, and M. Parrinello, *J. Chem. Theory Comput.*, 2005, **1**, 1176–1184.
18. The CP2K Developers Group, *cp2k.org*, 2012.
19. J. Moens, R. Seidel, P. Geerlings, M. Faubel, B. Winter, and J. Blumberger, *J. Phys. Chem. B*, 2010, **114**, 9173–9182.
20. S. Grimme, *J. Comput. Chem.*, 2006, **27**, 1787–1799.
21. M. Krack, *Theor. Chem. Acc.*, 2005, **114**, 145–152.
22. G. Lippert, J. Hutter, and M. Parrinello, *Theor. Chem. Acc.*, 1999, **103**, 124–140.
23. J. Vandevondele, M. Krack, F. Mohamed, M. Parrinello, T. Chassaing, and J. Hutter, *Comp. Phys. Comm.* 2005, **167**, 103–128.
24. J. Vandevondele and J. Hutter, *J. Chem. Phys.*, 2003, **118**, 4365.
25. J. Vandevondele and M. Sprik, *Phys. Chem. Chem. Phys.*, 2005, **7**, 1363–1367.
26. T. Laino and J. Hutter, *J. Chem. Phys.*, 2008, **129**, 074102.
27. P. P. Ewald, *Annalen der Physik*, 1921, **369**, 253–287.
28. J. Blumberger, *Phys. Chem. Chem. Phys.*, 2008, **10**, 5651–5667.
29. G. King and A. Warshel, *J. Chem. Phys.*, 1990, **93**, 8682–8692.
30. J. Blumberger and G. Lamoureux, *Mol. Phys.*, 2008, **106**, 1597–1611.
31. E. Vladimirov, A. Ivanova, and N. Rösch, *J. Chem. Phys.*, 2008, **129**, 194515.
32. W. Hoover, *Phys. Rev. A*, 1985, **31**, 1695–1697.
33. J. G. Kirkwood, *J. Chem. Phys.*, 1935, **3**, 300–313.
34. P. Kollman, *Chem. Rev.*, 1993, **93**, 2395–2417.
35. D. Shivakumar, Y. Deng, and B. Roux, *J. Chem. Theory Comput.*, 2009, **5**, 919–930.
36. A. V. Marenich, C. J. Cramer, and D. G. Truhlar, *J. Phys. Chem. B*, 2009, **113**, 6378–6396.
37. Y. Zhao and D. G. Truhlar, *Theor. Chem. Acc.*, 2008, **120**, 215–241.
38. J. J. Guerard and J. S. Arey, *J. Chem. Theory Comput.*, 2013, **9**, 5046–5058.
39. A. Lewis, J. A. Bumpus, D. G. Truhlar, and C. J. Cramer, *J. Chem. Educ.*, 2004, **81**, 596–604.
40. D. Ghosh, A. Roy, R. Seidel, B. Winter, S. E. Bradforth, and A. I. Krylov, *J. Phys. Chem. B*, 2012, **116**, 7269–7280.
41. R. Seidel, M. Faubel, B. Winter, and J. Blumberger, *J. Am. Chem. Soc.*, 2009, **131**, 16127–16137.
42. R. Ayala and M. Sprik, *J. Phys. Chem. B*, 2008, **112**, 257–269.